Electronic Supplementary Material (ESI) for Materials Chemistry Frontiers.

Supporting Information

Recyclable Amphiphilic Porous Thin Films as Electrodes for High-Performance Potassium-Ion Transport and Storage

Chuanting You[a⊥], *Weiwei Wei*[b, c⊥], *Jianyong Yu*[a], *Shichang Sun*[a], *Wei Xiao*[a], *Liwei Wang*[b], *Zhanhui Yuan*[a]*, *Fan Zhang*[c]*

[a]College of Materials Science and Engineering, Fujian Agriculture and Forestry University, Shangxiadian Road 15, 350002 Fuzhou, P. R. China
E-mail: zhanhuiyuan@fafu.edu.cn (Z. Y.)

[b]Ocean College, Minjiang University, Fuzhou 350108, P. R. China

[c]School of Chemistry and Chemical Engineering, Shanghai Jiao Tong University, Dongchan Road 800, 200240 Shanghai, P. R. China
E-mail: fan-zhang@sjtu.edu.cn (F. Z.)

[c]Ocean College, Minjiang University, Fuzhou 350108, P. R. China

[⊥]These authors contributed equally to this work.

Table of Contents

1 Experimental section:

1.1 Fabrication of the rGO/NFC thin film

The synthetic method of rGO/NFC thin film is exhibited in Figure 1a. As the shown in the figure, 210 mg NFC solution (1wt%) and 12 mg rGO powder (prepare via Hummers method) is added into 10 mL deionized water and fully stir for 10 min. The NFC solution (1 wt%) is an aqueous solution containing nanofibrillated cellulose (NFC) in a mass fraction of 1%. The NFC solution was prepared by slowly adding 1 g of NFC into 99 g of deionized water, and then fully stirred to form a uniform suspension. Then the NFC/rGO slurry was subject to continuous ultrasonic treatment for 3 h in 30 ℃-60 ℃ and had a rest for 1 h, this process was repeated over 5 times. Until a uniformly dispersed inky solution was formed, the NFC/rGO gelatinous thin film was prepared after filtration by using polytetrafluoroethylene (PTFE) membrane (0.22 μm pore diameter). The gelatinous film was dried at room temperature for over 24 h to form a flexible thin film called **85-rGO/NFC**. In the same way, using the above method and only changing the content of NFC in the composite to prepare different rGO/NFC films (is defined as *n*-rGO/NFC, n=65, 75, 85, and 90, n is represented the percentage of rGO in the composite).

1.2 Preparation of Lithium-ion, Sodium-ion, and Potassium-ion Supercapacitor

All these three kinds of symmetric supercapacitors were assembled with two flexible rGO/NFC films with same size as electrodes separated by one acetyl cellulose paper used as a separator to avoid short circuit. The difference is that they respectively used 1_M $LiPF_6$ in DMC, 1_M $NaPF_6$ in EC: DMC (1:1), and 1_M KPF_6 in EC: DMC: DEC (1:1:1) as electrolyte. To investigate the wettability of solvent in electrode, the contact angle of DMC, EC: DMC (1:1) and EC: DMC: DEC (1:1:1) on the surface of the **85-rGO/NFC** sample were monitored, respectively. These mixed solvents showed the similar wettability with the contact angles of about zero degree (Figure S10). Supercapacitors need to be assembled without water and oxygen in the glovebox.

1.3 Electrochemical Measurements

The electrochemical tests were carried out using an electrochemical station

(CHI660D, Shanghai) with symmetric supercapacitors at room temperature. Galvanostatic charge/discharge investigation was carried out in voltage range of 0-3 V with difference current density from 0.1 to 0.8 A cm^{-3}. Cyclic voltammetry was measured in the voltage range of 0-3 V at difference scan rates (5 mV s^{-1}, 10 mV s^{-1}, 20mV s^{-1}, 50 mV s^{-1}, and 100 mV s^{-1}). The electrochemical impedance spectroscopy (EIS) was performed at open circuit potential within a frequency range from 10^5 Hz to 10^{-2} at 0.5V.

Gravimetric specific capacitance (C_g) was calculated using the following equation (1) and (2)

$$C_g\,(\mathrm{F\ g^{-1}}) = A/(2msV) \quad (1)$$

$$C_g\,(\mathrm{F\ g^{-1}}) = I\,\Delta t / mV \quad (2)$$

where A is the area of CV curve, s is the scan rate of CV curve (V s^{-1}), V is the potential window (V), m is the mass of the electrodes (g), I is the current density (A g^{-1}), and Δt is the discharge time (s). The volumetric specific capacitance (C_v) was calculated by equation (3)

$$C_v\,(\mathrm{F\ cm^{-3}}) = \rho C_g \quad (3)$$

where ρ is the volumetric density of the films (g cm^{-3}), which was measured through equation (4)

$$\rho\ (\mathrm{g\ cm^{-3}}) = m / Sd \quad (4)$$

where m (g) is the dried electrode quality, S (cm^2) and d (cm) are the area and thickness of electrode. The volumetric energy density (E_v) and the power density (P_v) of electrode were calculated according to equation (5) and equation (6)

$$E_v\,(\mathrm{Wh\ L^{-1}}) = C_v V^2 / (2 \times 3.6) \quad (5)$$

$$P_v\,(\mathrm{W\ L^{-1}}) = 3600 \times E_v / \Delta t \quad (6)$$

where V is the potential window (V), and Δt is the discharge time (s)

1.4 Galvanostatic intermittent titration technique (GITT) measurements

The kinetics of lithium ion, sodium ion and potassium ion extraction/insertion in the **85-rGO/NFC** electrodes were measured by using the galvanostatic intermittent titration technique (GITT). The technique was be used to confirm the diffusion coefficient of Li^+ in Li_3Sb by Weppner and Huggins. By the ionic diffusion follows

Fick's second law, the diffusion can be calculated by the following equation.

$$D = \frac{4}{\pi\tau}\left(\frac{m\,V_M}{M\,S}\right)^2\left(\frac{\Delta E_S}{\tau\left(\Delta E_\tau / d\sqrt{\tau}\right)}\right)^2 \quad (\tau \ll L^2/D) \tag{7}$$

Where D is the diffusion coefficient of the ion; τ is the relaxation time; m is the mass of active matter; V_M is the molar volume; L is the electrodes' average thickness. Other parameters in the equation 6 can be defined in Figure S4.

Because a linear relationship exists between the voltage and $\tau^{1/2}$ in Figure S4, the equation 6 can be simplified as

$$D = \frac{4}{\pi\,\tau}\left(\frac{m\,V_M}{M\,S}\right)^2\left(\frac{\Delta E_S}{\Delta E_\tau}\right)^2 \tag{8}$$

For the GITT measurement (use Land system), the constant current density was set as 30 mA g^{-1} for a given time period (30 min), followed by an open-circuit stand for a specified time interval (60 min). The sequence was repeated until the target voltage was reached.

1.5 Material Characterization

The samples for tensile test were tailored into strip with the width of 5 mm and length of 15 mm by a bistoury. The testing was carried out via dynamic thermomechanical analysis (Q850, China) at room temperature. The morphology of rGO/NFC films was observed using Raman Imaging combined with Emission Scanning Electron Microscope (TESCAN-MAIA3, Czech). And the chemical element distribution of rGO/NFC electrodes after electrochemistry was detected using a FE-TEM (FEI Talos F200X) using an accelerating voltage of 200 kV. The rGO/NFC electrodes before electrochemistry and after electrochemistry were investigated by X-ray diffraction (XRD) using a Bruker D8 Advance diffractometer with Cu Kα radiation (≈1.54˚A) at 40 kV and 30 mA. Raman spectra were recorded on a RM2000 microscopic confocal Raman spectrometer employing a h14 nm laser beam. The X-ray photoelectron spectroscopy (XPS) analyses were performed an AXIS Ultra DLD (Kratos, Japan) photoelectron spectroscopy at 0.48 eV electronic resolution. Nitrogen adsorption/desorption isothermal was performed with a Micromeritics ASAP 2020 HD

Analyzer at 77 K. Pore size distribution was estimated based on BJH model.

2 Supplementary Figures

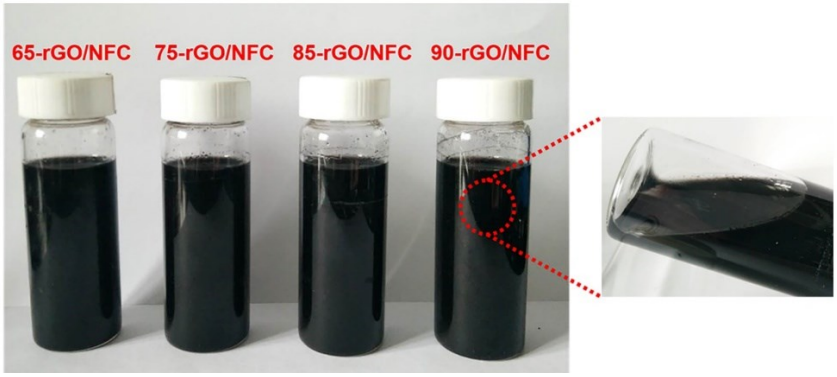

Figure S1. Digital images of rGO/NFC dispersion with different content of rGO and **90-rGO/NFC** after 48 hours.

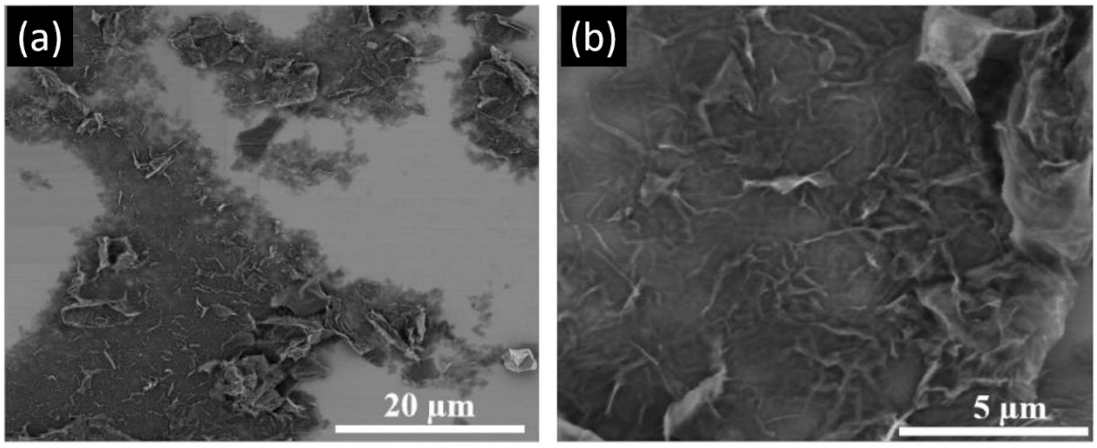

Figure S2. Scanning electron microscopy (SEM) images of NFC/rGO assembly dispersion solution.

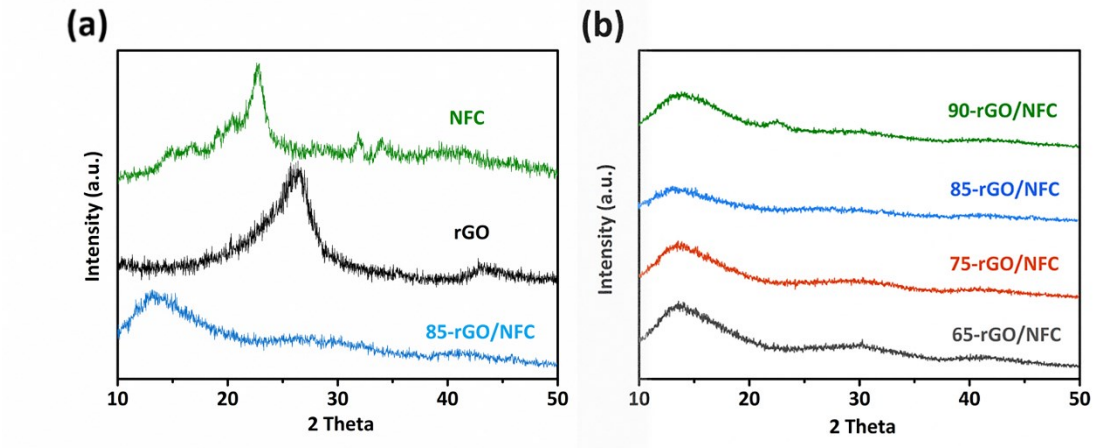

Figure S3. (a) XRD pattern of NFC, rGO and **85-rGO/NFC**. (b) XRD of the different films.

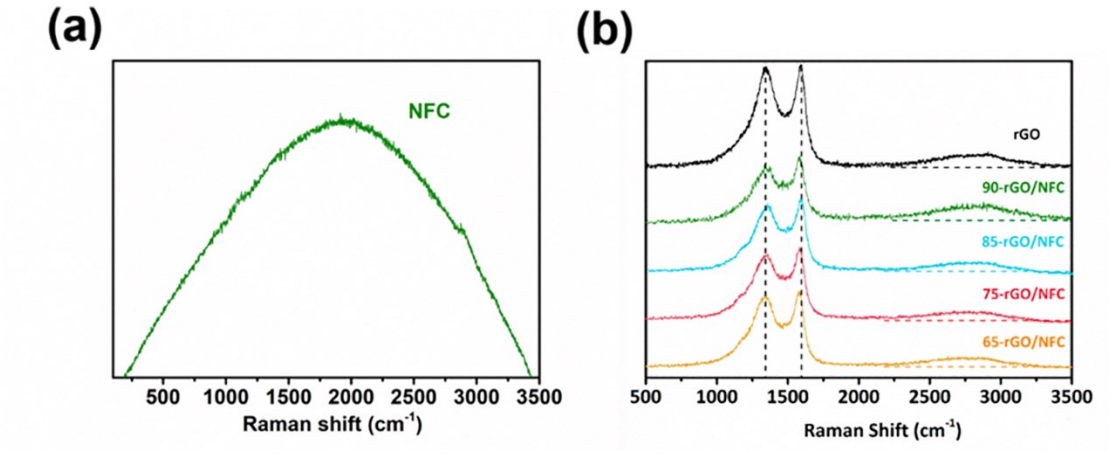

Figure S4. The Raman spectra of (a) NFC, (b) the neat rGO and the as-prepared ***n*-rGO/NFC** films.

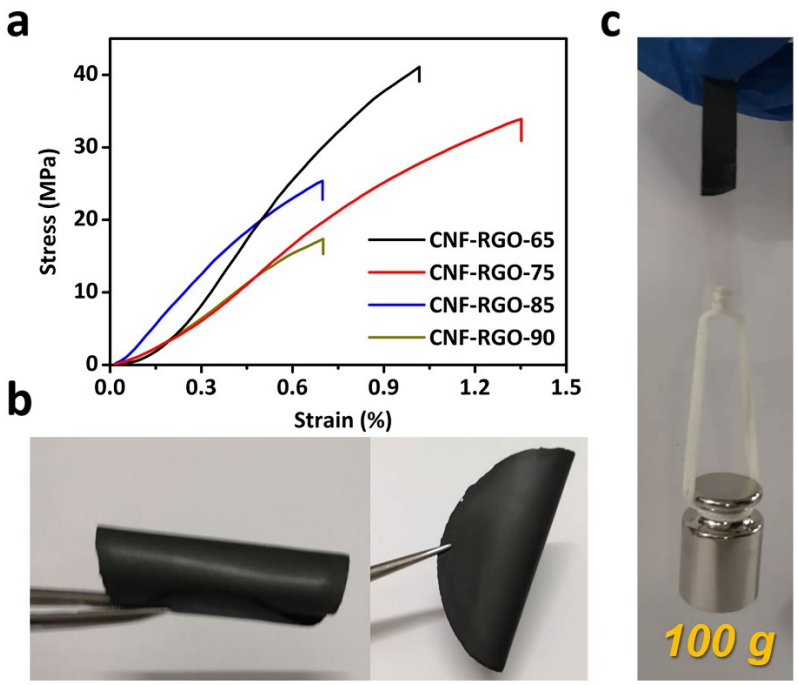

Figure S5. (a) Mechanical characters of ***n*-rGO/NFC**; (b-c) Reals images of reassembling film after being rolled, folded and bended.

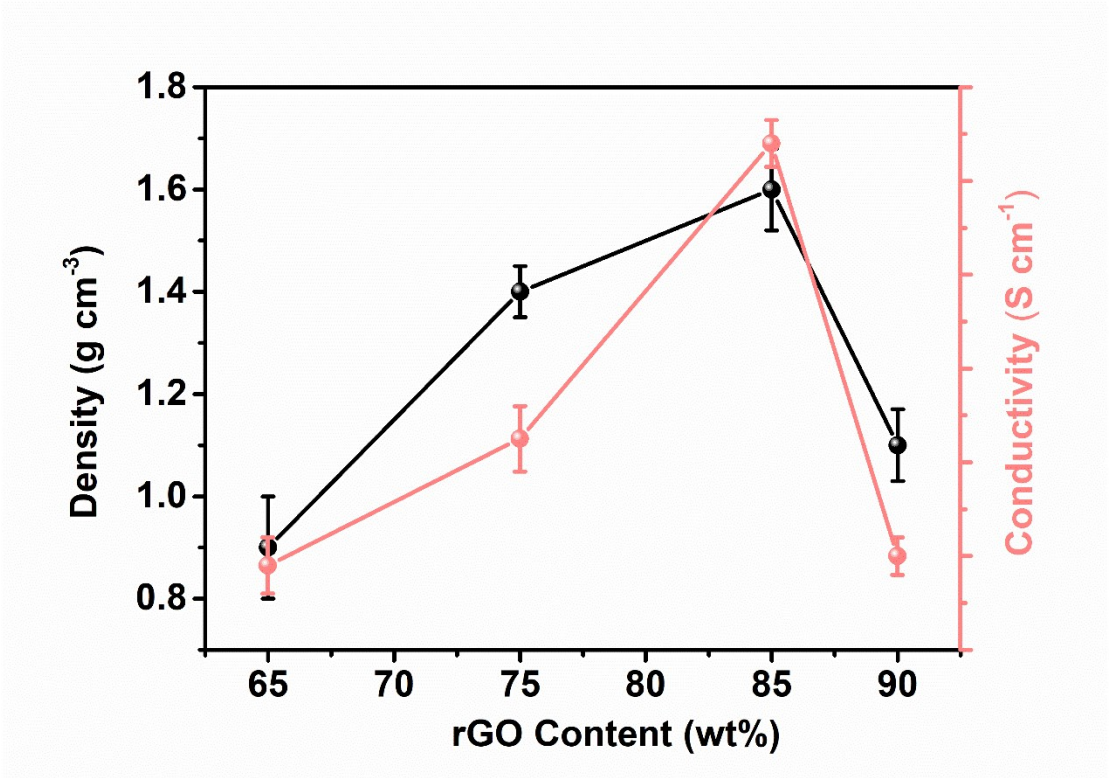

Figure S6. The variation tends of density and conductivity of ***n*-rGO/NFC** films.

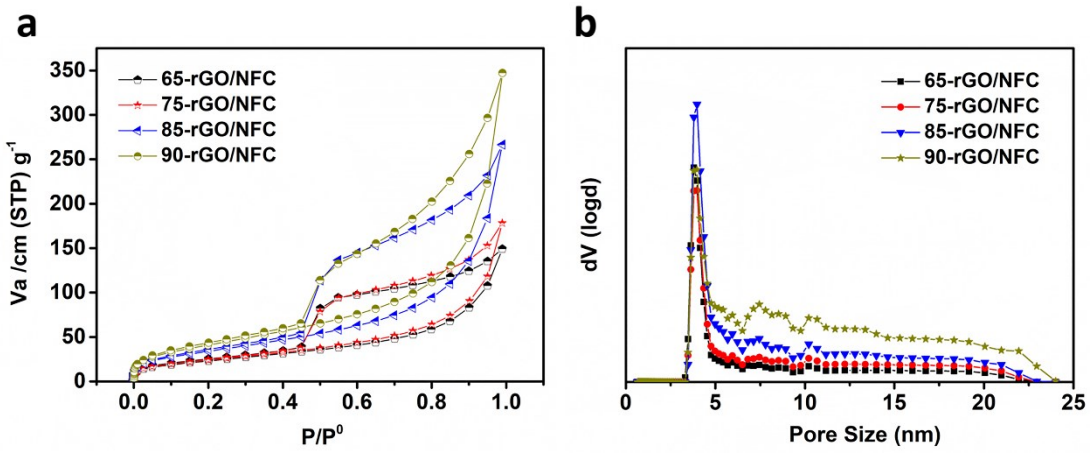

Figure S7. (a) N_2 adsorption-desorption isotherms and (b) The pore size distributions of ***n*-rGO/NFC**

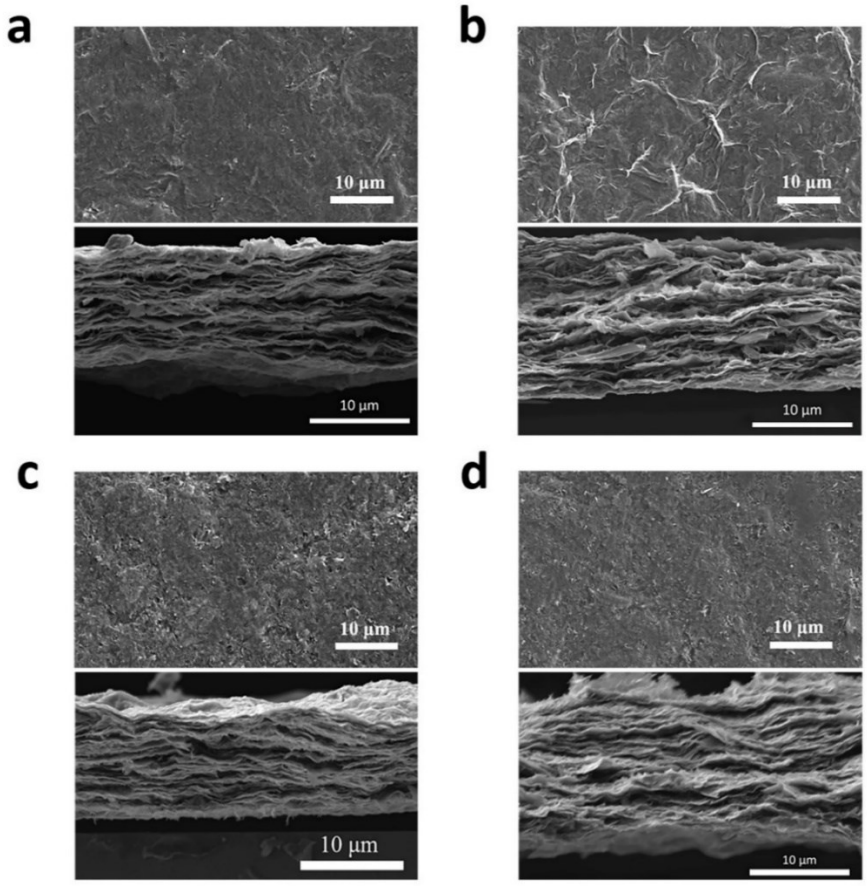

Figure S8. Top and side view of SEM images of different rGO/NFC weight ratio (a) **65-rGO/NFC**, (b) **75-rGO/NFC**, (c) **85-rGO/NFC** and (d) **90-rGO/NFC**, respectively.

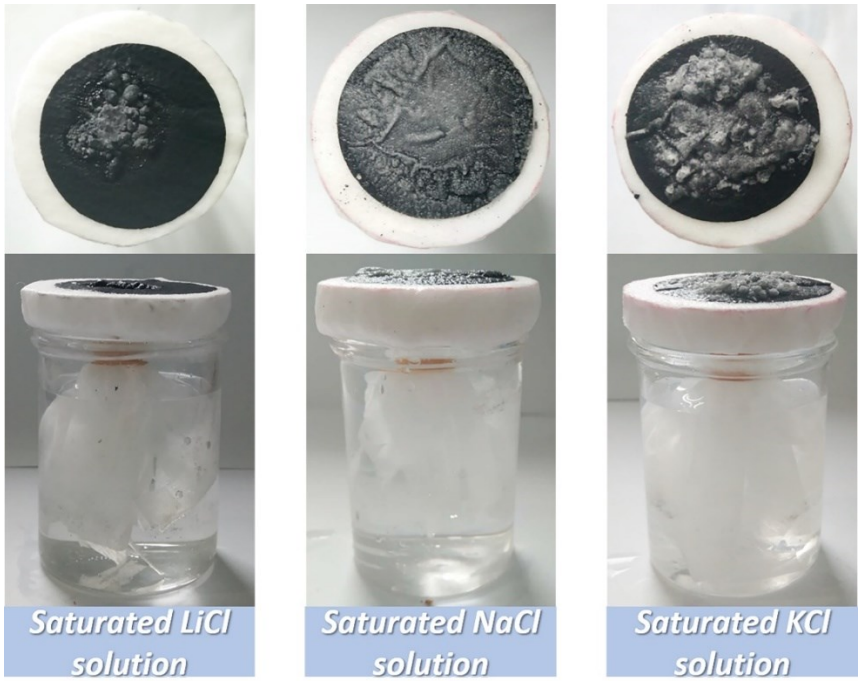

Figure S9. Digital photographs for appearing the crystalline salts of **85-rGO/NFC** with a substrate of airlaid paper, which were floated on crystalline salts appeared.

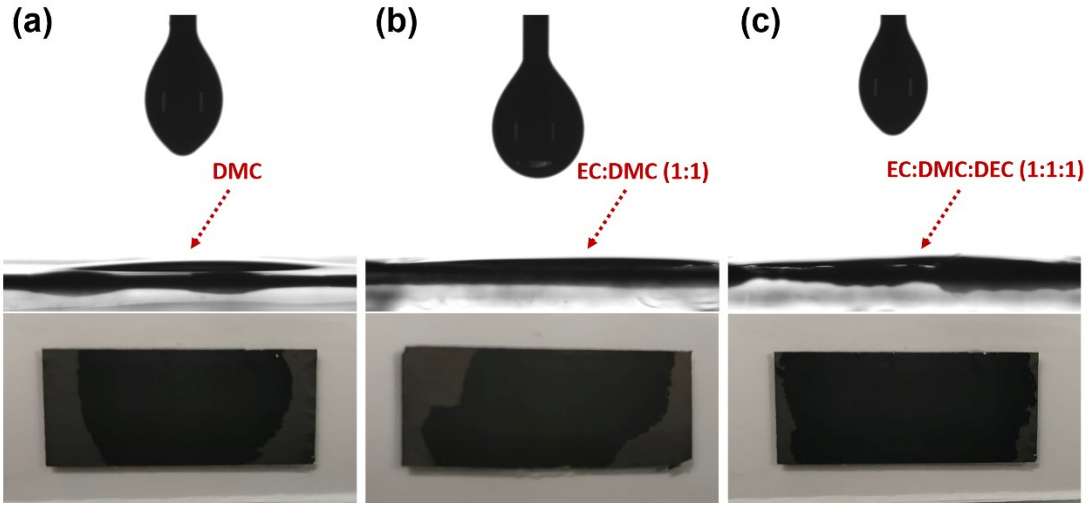

Figure S10. The wettability of the surface of **85-rGO/NFC** of difference solvent: (a) DMC (b) EC: DMC (1:1) and (c)EC: DMC: DEC (1:1:1).

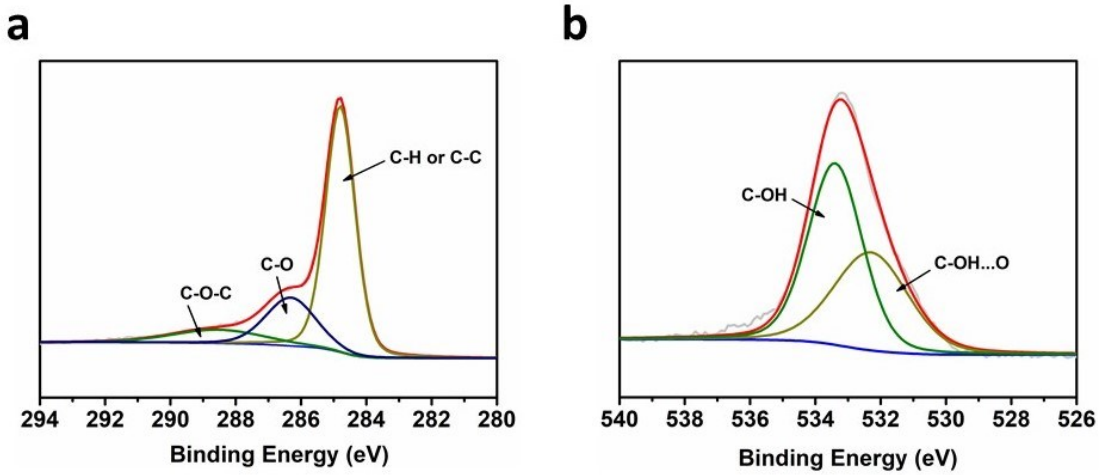

Figure S11. XPS spectra of **85-rGO/NFC** electrodes: (a) C 1s region (b) O 1s region

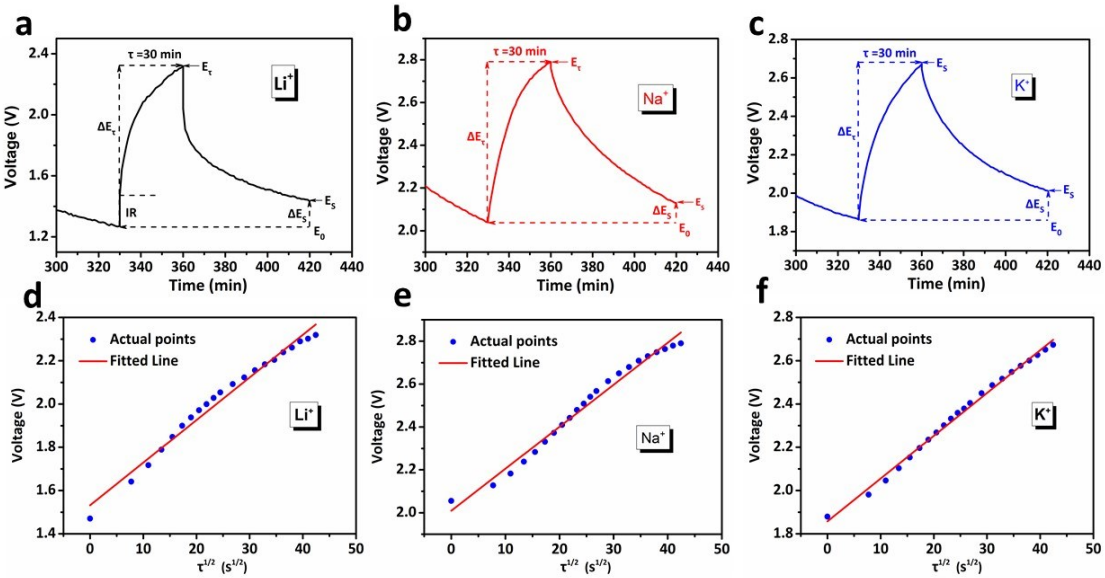

Figure S12. A single step of GITT of **85-rGO/NFC** electrode in the (a) $LiPF_6$, (b) $NaPF_6$ and (c) KPF_6 electrolyte. Linear behavior of voltage vs. $\tau^{1/2}$ relationship in GITT of the electrode in the (d) $LiPF_6$, (e) $NaPF_6$ and (f) KPF_6 electrolyte.

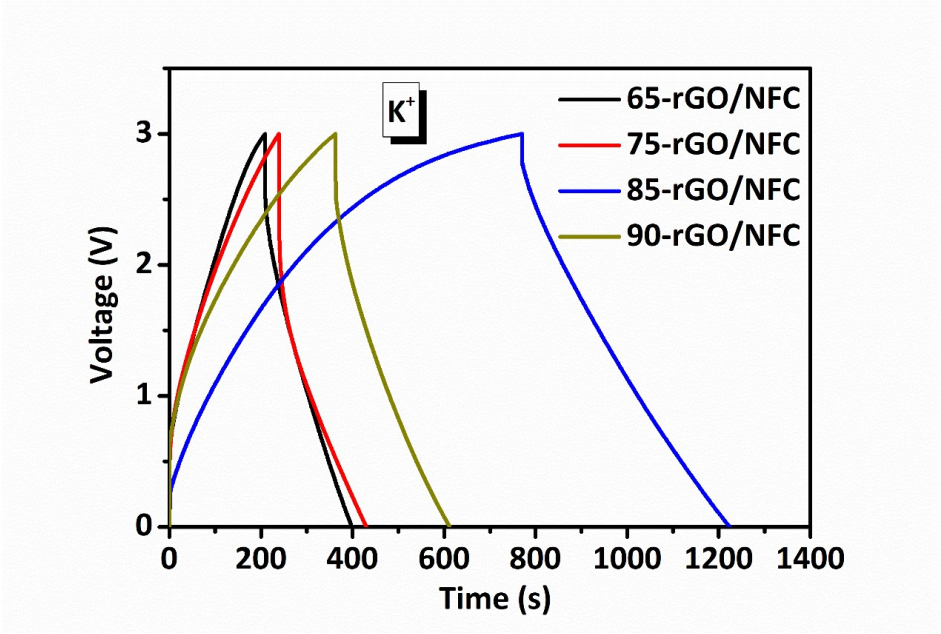

Figure S13. The GCD curves of ***n*-rGO/NFC** film electrodes (n=65, 75,85,90) at current density of 0.32 A cm^{-3} in the potassium ion-based capacitor.

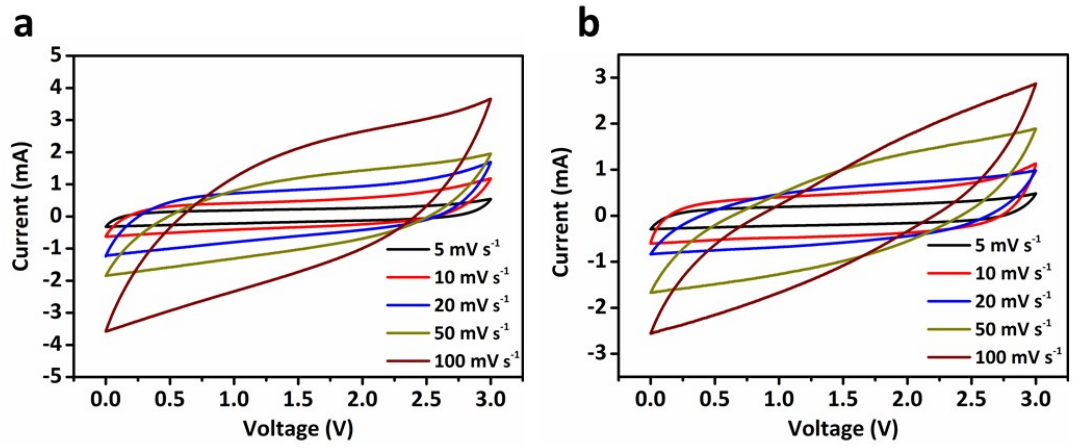

Figure S14. The CV curve of **85-rGO/NFC** at different scan rates in the (a) $LiPF_6$ and (b) $NaPF_6$ electrolyte.

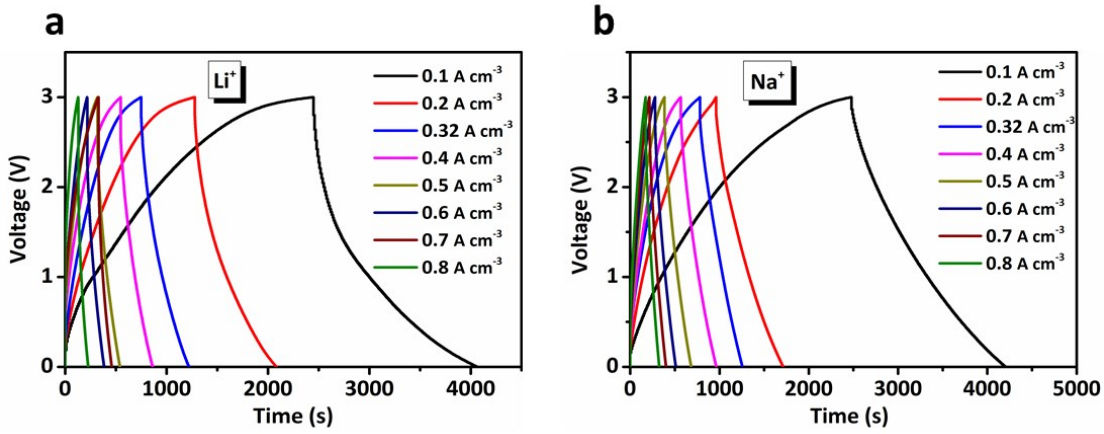

Figure S15. The GCD curve of **85-rGO/NFC** at different volumetric current densities in the (a) $LiPF_6$ and (b) $NaPF_6$ electrolyte.

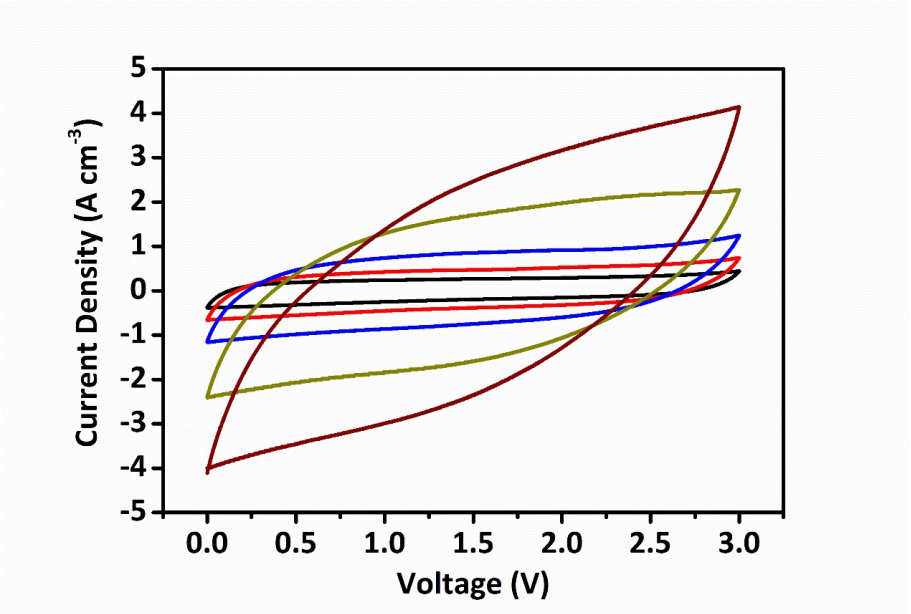

Figure S16. The CV curve of reassembling electrode at different scan rates in the KPF_6 electrolyte.

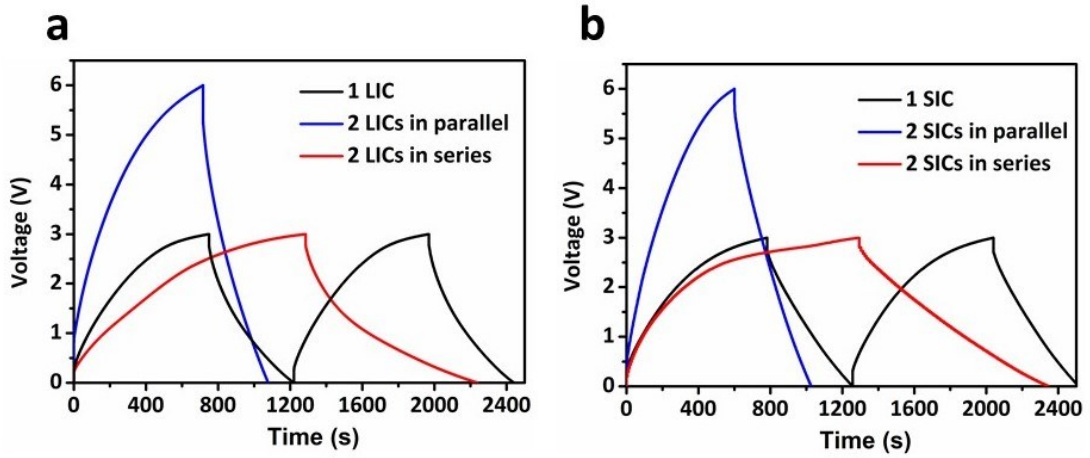

Figure S17. GCD profiles of single device and two devices in parallel and in series at a current density of 0.32 A cm^{-3}, respectively (a) lithium ion-based capacitor and (b) sodium ion-based capacitor

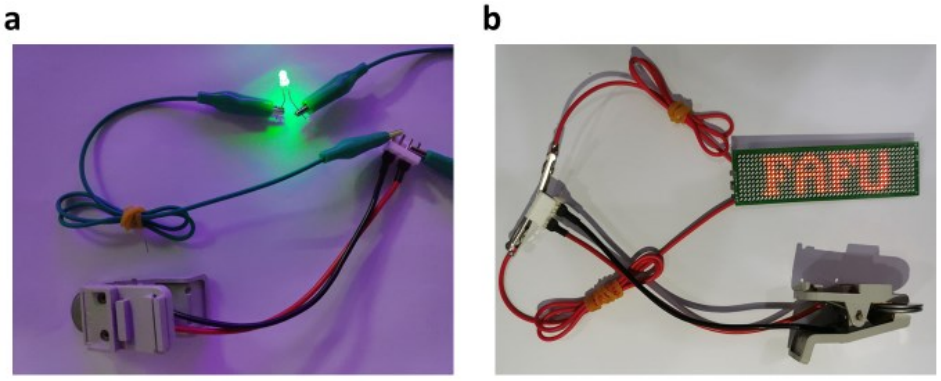

Figure S18. The digital photos of (a) a green LED scroller that is powered by device and (b) two MICs in series to power a LED scroller.

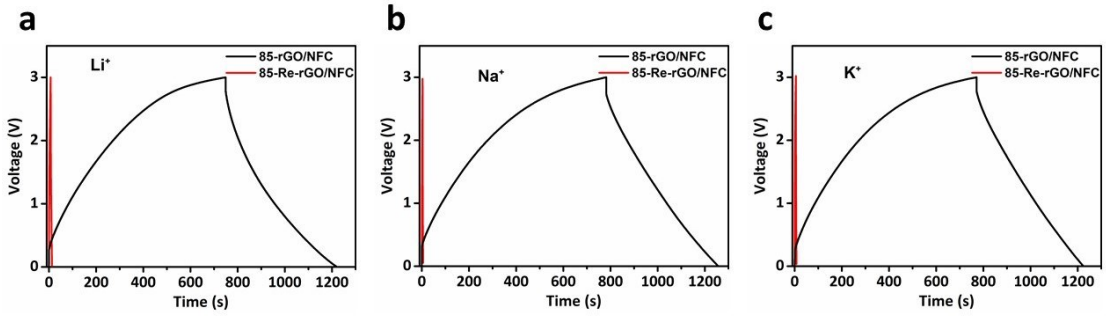

Figure S19. The GCD curve of **85-rGO/NFC** and **85-Re-rGO/NFC** at 0.32 A cm^{-3} in the (a) $LiPF_6$, (b) $NaPF_6$ and (c) KPF_6 electrolyte.

Table S1. Comparison of electrochemical performance between the ion supercapacitor used **85-rGO/NFC** electrodes and other supercapacitors used different electrodes.

Electrodes	Electrolyte	Voltage window (V)	Volumetric energy density (Wh L^{-1})	Volumetric power density (W L^{-1})	reference
85-rGO/NFC	$LiPF_6$	0-3	70	514	This work
	$NaPF_6$		74	560	
	KPF_6		67	552	
HPNC@NSs	$EMIMBF_4$	0-3.5	42.3	411	*ACS Nano*, 2015[1]
GH@NC@Co_9S_8	Alkaline	0-1.6	28.7	971.9	*J. Mater. Chem. A*, 2019[2]
Mxene@graphene	1M KCl	-0.7-0.3	32.6	74400	*Adv. Funct. Mater.*, 2017[3]
CNF@GO@MoO_3	PVDF–P407–[BMPY][NTf_2]	0-3.6	18.8	72.5	*J. Mater. Chem. A*, 2017[4]
PANI/RGO	PVA/H_2SO_4	0-1	8.8	30.77	*Adv. Mater.*, 2018[5]
NGMn	5 M LiCl	0-1.8	3.5	19	*ACS Appl. Mater. Interfaces*, 2016[6]
Nb_2O_5@AC	$LiPF_6$	1-3.5	6.7	374.6	*Adv. Funct. Mater.*, 2018[7]
2D-HPC	$EMIMBF_4$	0-4	8.4	24.9	*Adv. Mater.*, 2018[8]
Ni-MOF@AC	3M KOH	0-1.2	4.18	231.2	*J. Mater. Chem. A*, 2016[9]
$Ni_{0.25}Mn_{0.75}O$@C	PVA-LiCl	0-1.4	4.72	776	*Adv. Mater.*, 2017[10]
Carbon cloth	PVA/H_2SO_4	-0.5-1	4.27	1320	*ACS Appl. Mater. Interfaces*, 2019[11]
Nb_2O_5@CNF	$NaPF_6$	0-4	11.2	5400	*Small*, 2019[12]
BP@CNT	PVA/H_3PO_4	0-1	5.71	11000	*ACS Appl. Mater. Interfaces*, 2017[13]

Reference

1. C. C. Jianhua Hou, Faryal Idrees, and Xilan Ma, *ACS Nano*, 2015, **9-3**, 2556.
2. H. Niu, Y. Zhang, Y. Liu, B. Luo, N. Xin and W. Shi, *J. Mater. Chem. A*, 2019, **7**, 8503.
3. J. Yan, C. E. Ren, K. Maleski, C. B. Hatter, B. Anasori, P. Urbankowski, A. Sarycheva and Y. Gogotsi, *Adv. Funct. Mater.*, 2017, **27**, 1701264.
4. Q. Zheng, A. Kvit, Z. Cai, Z. Ma and S. Gong, *J. Mater. Chem. A*, 2017, **5**, 12528.
5. P. Li, Z. Jin, L. Peng, F. Zhao, D. Xiao, Y. Jin and G. Yu, *Adv. Mater.*, 2018, **30**, e1800124.
6. Y. Liu, X. Miao, J. Fang, X. Zhang, S. Chen, W. Li, W. Feng, Y. Chen, W. Wang and Y. Zhang, *ACS Appl. Mater. Interfaces*, 2016, **8**, 5251.
7. B. Deng, T. Lei, W. Zhu, L. Xiao and J. Liu, *Adv. Funct. Mater.*, 2018, **28**, 1704330.
8. L. Yao, Q. Wu, P. Zhang, J. Zhang, D. Wang, Y. Li, X. Ren, H. Mi, L. Deng and Z. Zheng, *Adv. Mater.*, 2018, **30**, 1706054.
9. Y. Yan, P. Gu, S. Zheng, M. Zheng, H. Pang and H. Xue, *J. Mater. Chem. A*, 2016, **4**, 19078.
10. W. Zuo, C. Xie, P. Xu, Y. Li and J. Liu, *Adv. Mater.*, 2017, **29**, 1703463.
11. Z. Miao, Y. Huang, J. Xin, X. Su, Y. Sang, H. Liu and J. J. Wang, *ACS Appl. Mater. Interfaces*, 2019, **11**, 18044.
12. Y. Li, H. Wang, L. Wang, Z. Mao, R. Wang, B. He, Y. Gong and X. Hu, *Small*, 2019, **15**, 1804539.
13. B. Yang, C. Hao, F. Wen, B. Wang, C. Mu, J. Xiang, L. Li, B. Xu, Z. Zhao, Z. Liu and Y. Tian, *ACS Appl. Mater. Interfaces*, 2017, **9**, 44478.